






Article

Frequency Response Analysis for Three-Phase Star and Delta Induction Motors: Pattern Recognition and Fault Analysis Using Statistical Indicators

Salem Mgamal Al-Ameri ^{1,2}, Zulkurnain Abdul-Malek ¹, Ali Ahmed Salem ^{1,*},
Zulkurnain Ahmad Noorden ¹, Ahmed Allawy Alawady ^{3,4}, Mohd Fairouz Mohd Yousof ⁴,
Mohamed Ibrahim Mosaad ⁵, Ahmed Abu-Siada ⁶ and Hammam Abdurabu Thabit ⁷

- ¹ Institute of High Voltage and High Current, School of Electrical Engineering, Universiti Teknologi Malaysia, Johor Bahru 81310, Malaysia
² Department of Electrical & Computer Engineering, Curtin University Malaysia, Miri 98009, Malaysia
³ College of Technical Engineering, The Islamic University, Najaf 54001, Iraq
⁴ Faculty of Electrical and Electronic Engineering, Universiti Tun Hussein Onn Malaysia, Parit Raja 86400, Malaysia
⁵ Electrical Engineering Department, Faculty of Engineering, Damietta University, Damietta 34517, Egypt
⁶ Electrical and Computer Engineering Department, Curtin University, Bentley, WA 6152, Australia
⁷ School of Physics, Universiti Sains Malaysia, George Town 11800, Malaysia
* Correspondence: ahmedali.a@utm.my



Citation: Al-Ameri, S.M.; Abdul-Malek, Z.; Salem, A.A.; Noorden, Z.A.; Alawady, A.A.; Yousof, M.F.M.; Mosaad, M.I.; Abu-Siada, A.; Thabit, H.A. Frequency Response Analysis for Three-Phase Star and Delta Induction Motors: Pattern Recognition and Fault Analysis Using Statistical Indicators. *Machines* **2023**, *11*, 106. <https://doi.org/10.3390/machines11010106>

Academic Editors: Te Han, Ruonan Liu, Zhibin Zhao and Pradeep Kundu

Received: 26 November 2022
Revised: 5 January 2023
Accepted: 9 January 2023
Published: 13 January 2023



Copyright: © 2023 by the authors. Licensee MDPI, Basel, Switzerland. This article is an open access article distributed under the terms and conditions of the Creative Commons Attribution (CC BY) license (<https://creativecommons.org/licenses/by/4.0/>).

Abstract: This paper presents a new investigation to detect various faults within the three-phase star and delta induction motors (IMs) using a frequency response analysis (FRA). In this regard, experimental measurements using FRA are performed on three IMs of ratings 1 HP, 3 HP and 5.5 HP in normal conditions, short-circuit fault (SC) and open-circuit fault (OC) conditions. The SC and OC faults are applied artificially between the turns (Turn-to-Turn), between the coils (Coil-to-Coil) and between the phases (Phase-to-Phase). The obtained measurements show that the star and delta IMs result in dissimilar FRA signatures for the normal and faulty windings. Various statistical indicators are used to quantify the deviations between the normal and faulty FRA signatures. The calculation is performed in three frequency ranges: low, middle and high ones, as the winding parameters including resistive, inductive and capacitive components dominate the frequency characteristics at different frequency ranges. Consequently, it is proposed that the boundaries for the used indicators facilitate fault identification and quantification.

Keywords: induction motors (IMs); frequency response analysis (FRA); pattern recognition; fault detection; statistical indicators

1. Introduction

Induction motors (IMs) represent key components for sustainable industrial production lines. IMs are subjected to continuous mechanical and thermal stresses during operation, which makes them more prone to wear and tear and insulation degradation. The insulation degradation of the windings, if it is not detected and rectified at an early stage, leads to short-circuit faults and potential consequences, including production line interruptions. Statistical studies show that bearing and stator winding faults represent the highest percentage of faults among the IMs (41% and 37%, respectively) [1]. Another survey shows that stator windings represents 26% of the IM failure causes [2]. Therefore, investigating the IM condition is essential to avoid serious damage to the unit. In [3,4], several conventional tests were used to evaluate the health condition of IMs such as the Partial Discharge (PD), tan delta (TD) and stator current signature. Other methods include the Park's vector modulus (PVM) in [5], and the discrete wavelet transform (DWT), simulation and experimental under load and no-load measurements, and a variety of other

methods in [6,7]. The fact is that scenarios in which the above methodologies are used are not common in practice.

FRA has been widely used to assess the mechanical integrity of power transformers [8]. The FRA method measures the frequency characteristics of the winding transfer function in the FRA range from 10 Hz to 2 MHz [9–12]. Mechanical deformation within the magnetic core and winding faults alters the reference frequency characteristics from which various faults can be identified and quantified [13,14]. While much attention has been paid by researchers to investigate the application of FRA on power transformers, only a few studies have presented the application of FRA to detect the faults within rotating machines such as IMs, as summarized below:

- In [15], the results show that the FRA method can be utilized to identify faults in the IMs. The FRA measurement shows a noticeable variation in the frequency range of between 1 kHz and 300 kHz due to broken bars in the squirrel cage rotor. The investigation was based on the rotor's position. Additionally, no FRA interpretation methodology was presented.
- The findings in [16] show that short-circuit (SC) faults result in a variation on the IM FRA signature with significant variation due to Phase-to-Phase SC faults. Three statistical indicators were only used to interpret the obtained results, and only two types of SC faults were investigated.
- In [17], the conducted study shows that FRA can detect emerging IM winding faults at the 1% fault level. The SC fault in the turns in only one phase was studied. Additionally, there is a lack of results interpretation.
- The research in [18,19] shows that FRA could be an alternative offline method used to diagnose SC faults in three-phase IMs. The results were analysed using the assessment factor E12, which may not give a clear image of the IM condition.
- In [20], the results show that FRA detects the variation due to IM winding faults. The interpretation of the measured data was conducted using statistical indicators along with personnel experience.
- In [21], FRA measurements of the power transformer and IM are taken. While the measurement procedure is proposed for IM, no interpretation methodology was proposed in this paper.
- In [22], the study was conducted to evaluate the application of FRA on the SC fault assessment of synchronous machines. The FRA curve was obtained to show the changes due to the SC fault. In the study, small- and medium-sized machines were tested.

Even though the FRA method that is used to detect faults within IMs has been used before, there are no detailed studies on the measurement setup nor the effect of different IM winding connections on the FRA signature. Additionally, the detailed interpretation and pattern recognition of the IM FRA signatures has not been given much attention yet. In this research, the FRA patterns have been obtained for the star and delta connection. Additionally, the FRA patterns are measured in normal and short-circuit conditions.

In this paper, the FRA patterns for the star (Y) and delta (Δ) connection of the IM stator winding with SC and open-circuit (OC) faults are measured and analyzed. Measurements are taken of three IMs of different ratings: 1 HP, 3 HP and 5.5 HP. Statistical indicators are employed to quantify the difference between the faulty and healthy FRA signatures and to identify the threshold limits for each indicator over three frequency ranges. Thus, the key contributions of this research paper can be summarized as:

- We measured and compared the FRA patterns of the star and delta stator winding for three IMs of different sizes.
- We investigated the effect of SC and OC faults of star and delta IM windings on the FRA signature.
- We identified the threshold limits for various statistical indicators to facilitate the reliable identification and quantification of IM windings faults using FRA measurements.

Owing to the fact that FRA is mainly a graphical analysis-based technique, a visual inspection can be used to detect the variations between the IM FRA signature and its reference signature, which should be measured under normal motor conditions. Furthermore, various statistical metrics can be used to quantify the variation between the two FRA signatures [23–25]. There are more than ten statistical indicators that have been successfully used to detect the variation between the two datasets. For instance, the correlation coefficient (CC) metric becomes 1 if the two datasets are identical, while it reduces to 0 when there are significant variations between the two datasets [26]. The absolute sum of logarithmic error (ASLE) is 0 when there is no variation between the two FRA datasets [25,27,28]. The standard deviation (SD) has a similar trend as that of the ASLE and sensitivity to variations in the FRA data sets [23]. The mean squared error (MSE) was used in [24,29]. In this regard, the drawback of employing statistical indicators to analyse the FRA data is that there is no approved benchmarking. For further benefits to using the statistical indicators, the benchmarking or boundary limits can be identified to facilitate reliable fault identification and quantification.

The rest of the paper is organized as below:

Section 2 presents the FRA measurement setup for the investigated IMs. In Section 3, the FRA measurement results are presented and analysed for three case studies. In Section 4, the FRA results are analysed using several statistical indicators. The further discussion and comparison of the FRA patterns for the star and delta connections are available in Section 5. Lastly, the most important conclusions are illustrated in Section 6.

2. Setup and FRA Measurement

The common SC faults within three-phase stator windings include SCs between the turns in the same phase (Turn-to-Turn), SCs between the coils in the same phase (Coil-to-Coil) and SCs between the phases (Phase-to-Phase), which may be between the turns or the coils [26].

The FRA measurement has been conducted on three IMs, whose specifications are listed in Table 1. A commercial FRA analyzer is used to inject a low AC voltage ($V_{in} < 20$ V) at a wide frequency range at one terminal of each phase. The output voltage, ' V_{out} ', is measured at the other terminal of the same phase or at another phase terminal. The frequency response is usually expressed as the transfer function ' HF ' from (V_{out}) to (V_{in}), and it is plotted as the magnitude in dB , as given by (1) and (2). The magnitude plot can provide sufficient information about the condition of the electric machine [27].

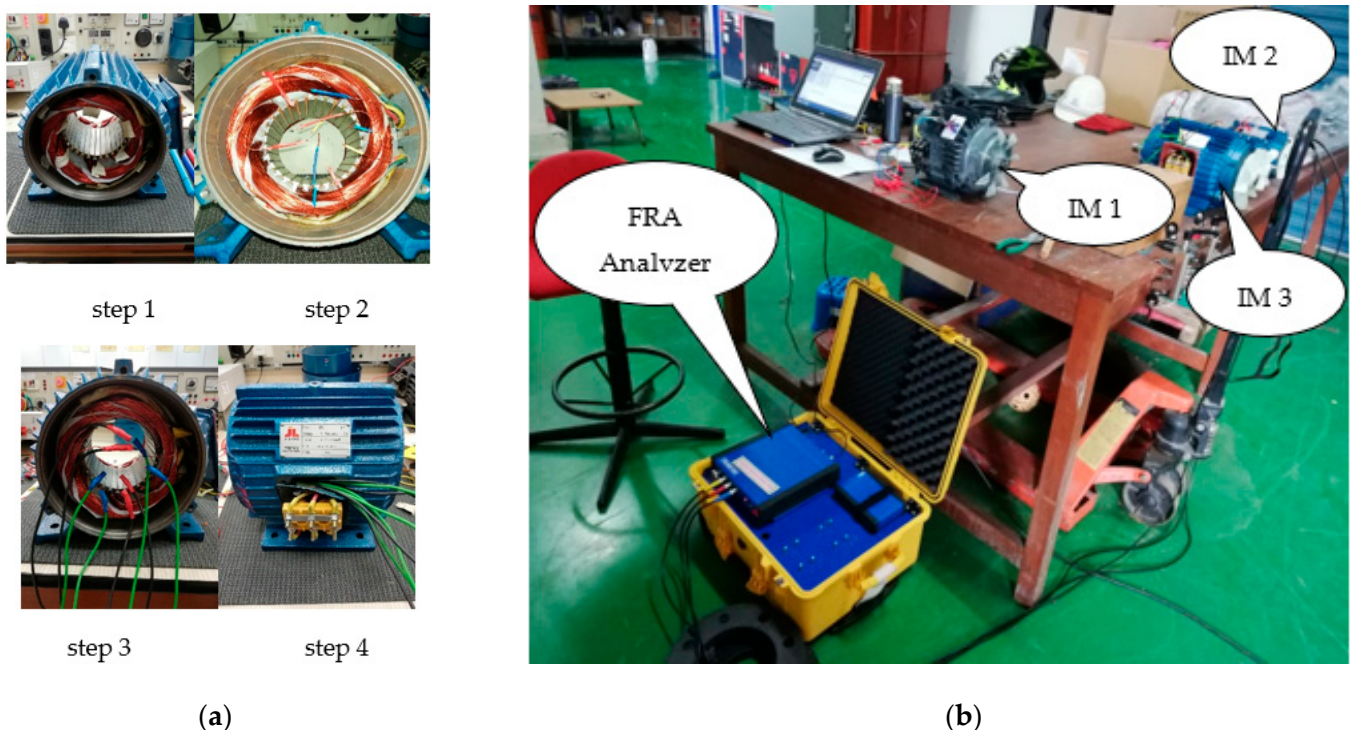
$$HF = \frac{V_{out}}{V_{in}} \quad (1)$$

$$Magnitude \text{ dB} = 20 \log_{10} \frac{V_{out}}{V_{in}} \quad (2)$$

The SC faults are performed on the star connection at one phase and from phase to phase. Additionally, the delta connection measurement is taken in a similar way. The steps of developing the faults are presented in Figure 1a. In step 1, the motor is dismantled, and the motor phases are determined. In step 2, the wire terminals from the winding have been extended to where the fault will be created. In step 3, the wire terminal is extended with suitable extensions, and in step 4, the wire extensions are labelled for performing the FRA measurement. The SC and OC faults form, and the FRA measurements are performed on the three selected IMs, which are shown in Figure 1b. The faults introduced at the minimum number of windings show the effect on the FRA measurement. The FRA measurement was conducted with no rotor effect. At this stage, the obtained FRA patterns for the motors are compared between the normal and faulty stator windings without a rotor. So, the changes and variations of the response are due to the faulty winding only.

Table 1. Specifications data of the three IMs selected for the FRA laboratory measurements.

Motor	Motor 1	Motor 2	Motor 3
Rotor speed	1500 rpm	2840 rpm	2880 rpm
Made	JILANG	JILANG	JILANG
Model	110RK-3DS	Y90L-2	Y112M-2
No. Phases	3-Ph	3-Ph	3-Ph
Rated power	0.75 kW/1HP	2.2 kW/3 HP	4 kW/5.5 HP
Rated Voltage	415 V/50 Hz	415 V/50 Hz	415 V/50 Hz
Current	7.5 A	8.83 A	8.17 A
Efficiency	73%	80.5%	85.5%
Power factor	0.76	0.86	0.87

**Figure 1.** Measurement setup in the laboratory. (a) SC and OC faults development. (b) Measurement connections.

Motors of different sizes and specifications are chosen, as shown in Table 1. The selected motors are widely used in the several kinds of machinery purposes such as fans, pumps, machine tools, compressors, gearboxes, and transportations. The motors winding specification/geometries data are provided in Table 1, and they significantly affected the measurement results [30,31].

Figure 2 shows the overview of the measurement and research investigation process. In Activity 1, the FRA measurement is taken during one phase of the star and delta connections before and after developing the faults. In Activity 2, a comparison process using visual and statistical indicators is conducted on the FRA patterns of the star and delta connections under normal and faulty conditions. In Activity 3, the comparable faults with similar effects are clustered, and the dissimilar patterns are separated.

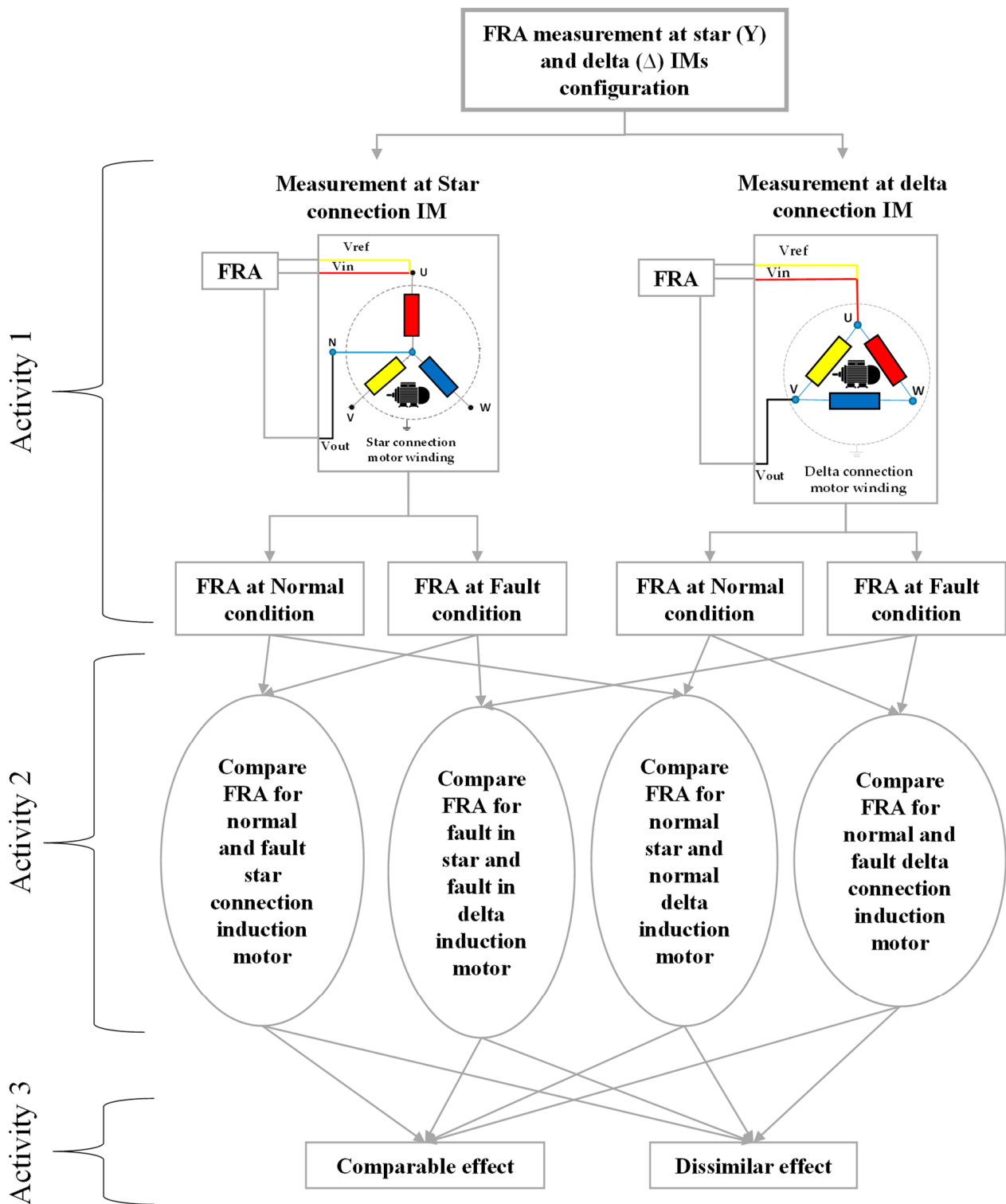


Figure 2. The measurement setup and results comparison process methodology.

3. FRA Results

The FRA measurement was obtained from three different IM sizes. The FRA measurement is sensitive to the physical structure of the winding. Therefore, this study was conducted on 1 HP, 3 HP and 5.5 HP induction motors. The FRA measurements are taken in one phase for all of the cases. In all of the obtained FRA plots, the solid line represents

the winding signature in the normal conditions, while the dotted lines present the faulty signatures. The investigated case studies on the three IMs are presented below.

3.1. One HP Induction Motor

The FRA measurement results shown in Figure 3 represent the FRA signatures of Phase A of this IM in normal and faulty conditions for the star and the delta stator windings. It can be observed that the FRA signature for healthy Y winding has a higher magnitude than the corresponding signature does for the Δ winding, with a first resonant frequency that is shifted slightly to the left in the case of Y winding. This is attributed to the variation in the magnetic flux distribution among the two winding connections in the low-frequency range. Overall, the trend of the FRA signatures of both of the windings is alike in the entire frequency range.

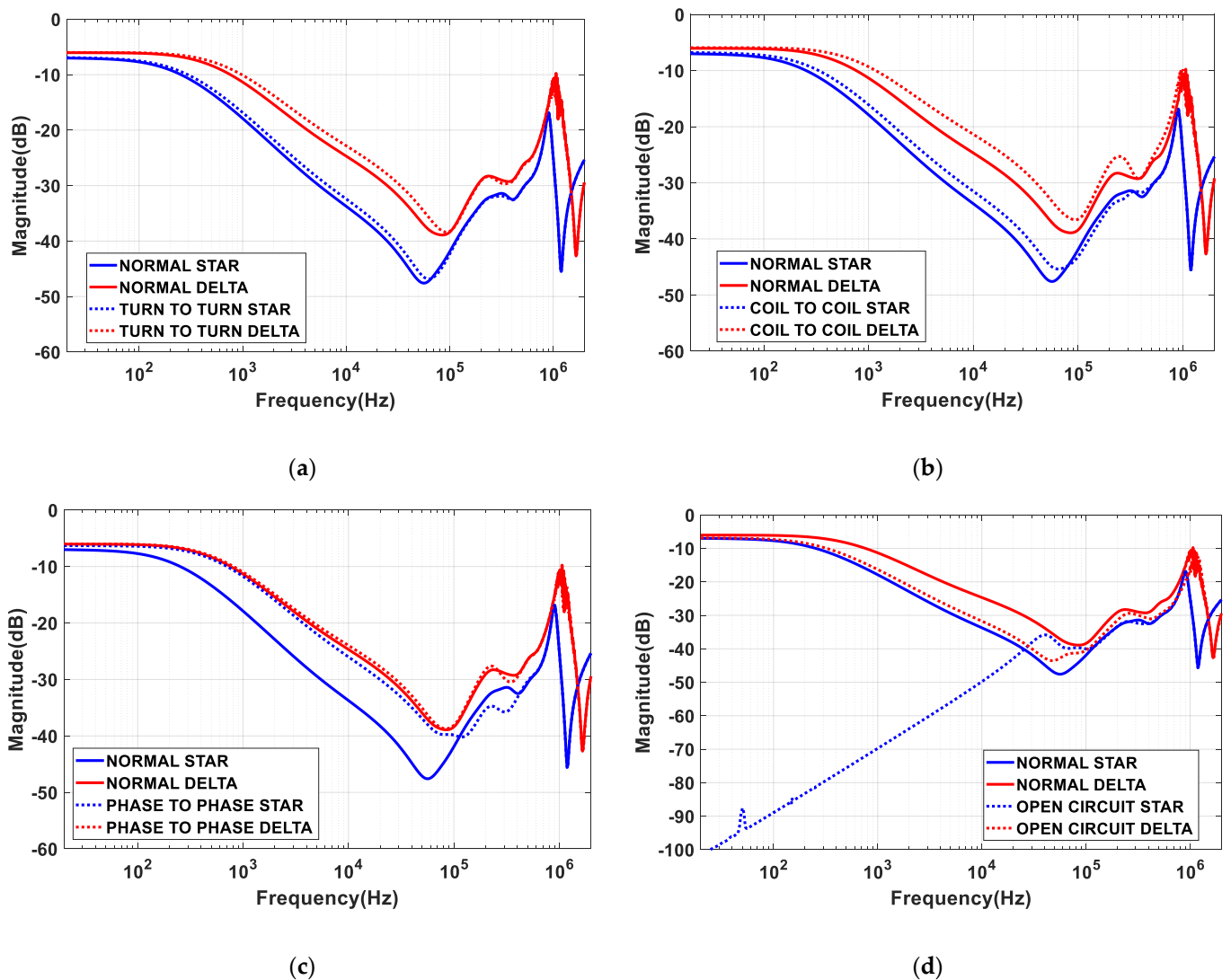


Figure 3. FRA measured responses for star vs. delta of 1 HP IM at (a) Normal vs. Turn-to-Turn, (b) Normal vs. Coil-to-Coil, (c) Normal vs. Phase-to-Phase SC fault and (d) Normal vs. open circuits.

Figure 3a shows that the Turn-to-Turn fault exhibits an almost similar effect on the star and delta connections. The response shows an increase in the magnitude and shifts towards the higher frequencies in the frequency range from 1 kHz to 100 kHz. As shown in Figure 3b, the Coil-to-Coil fault has a similar impact on the FRA signature as that of the Turn-to-Turn fault, but there is a more observable change in the magnitude in the frequency range from 1 kHz to 1 MHz. In the frequency range from 100 kHz to 300 kHz, the trends of

the FRA traces due to the Coil-to-Coil fault in the star and delta connections with respect to the normal signature are opposite to each other, i.e., it increases in the case of the Y winding, and it decreases in the case of the Δ winding.

Figure 3c Shows the effect of Phase-to-Phase short-circuit fault on the FRA signatures of both Y- and Δ windings. While the impact is significant on the Y winding is shown in 20 Hz to 300 kHz, it is very slight in the case of Δ winding as can be observed in the frequency range 1 kHz to 300 kHz.

As shown in Figure 3d, the open-circuit fault in the star connection results in a substantial drop in the response magnitude from 20 Hz to 50 kHz, while it introduces a slight drop in the magnitude in the case of delta connection in the frequency range from 100 Hz to 1 MHz.

3.2. Three HP Induction Motor

Figure 4a shows a comparable trend for the Turn-to-Turn fault in the star and delta connections. Similar to the above case study, there is an increase in the magnitude in the frequency range from 1 kHz to 1 MHz. However, the variation in the faulty signature from the reference one is more observable in the high-frequency range when it is compared with that of the above case study. This may be attributed to the higher rating of this motor.

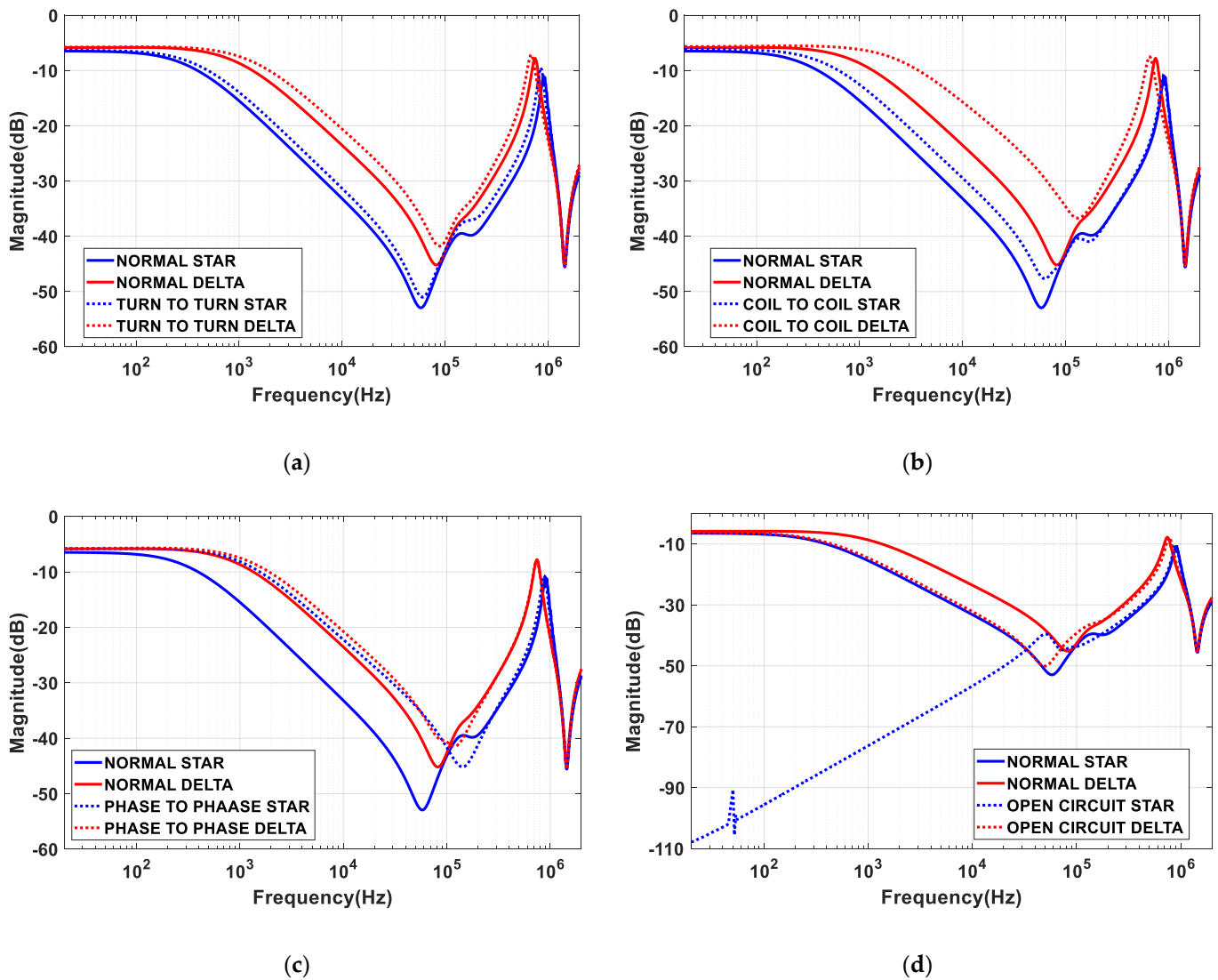


Figure 4. FRA measured responses for star vs. delta 3 HP IM at (a) Normal vs. Turn-to-Turn, (b) Normal vs. Coil-to-Coil, (c) Normal vs. Phase-to-Phase SC fault and (d) Normal vs. open circuit.

The Coil-to-Coil fault introduces more variation into the FRA signature for both of the windings compared to that of the Turn-to-Turn fault, as shown in Figure 4b. There is a huge decrease in the response magnitude in the frequencies from 1 kHz to 1 MHz for the delta connection IM. In the frequencies from 100 kHz to 300 kHz, the Coil-to-Coil fault exhibits dissimilar effects for the delta and star windings, as observed in the above case study as well.

Figure 4c shows that the Phase-to-Phase fault introduces a significant variation in the response for the star connection. The massive decrease in the magnitude and the shifting to high frequencies can be noted in the frequency range from 20 Hz to 300 kHz. In the delta connection, the FRA trace of the faulty winding does not show a major deviation as it does in the star connection, and a small reduction of the response magnitude from 1 kHz to 300 kHz can be noticed.

For the open-circuit fault shown in Figure 4d, the FRA signature of the faulty winding in the star connection shows a huge drop in the response magnitude in the frequency range from 20 Hz to 50 kHz. However, the response due to the open-circuit fault in the delta connection just shows an average drop in the frequency range from 100 Hz to 80 kHz.

3.3. Five Point Five HP Induction Motor

As shown in Figure 5a, the Turn-to-Turn fault for the 5.5 HP IM has a similar impact on the FRA signature, as in the above two cases, as it increases the response magnitude in the frequencies from 1 kHz to 100 kHz for both the star and delta winding connections.

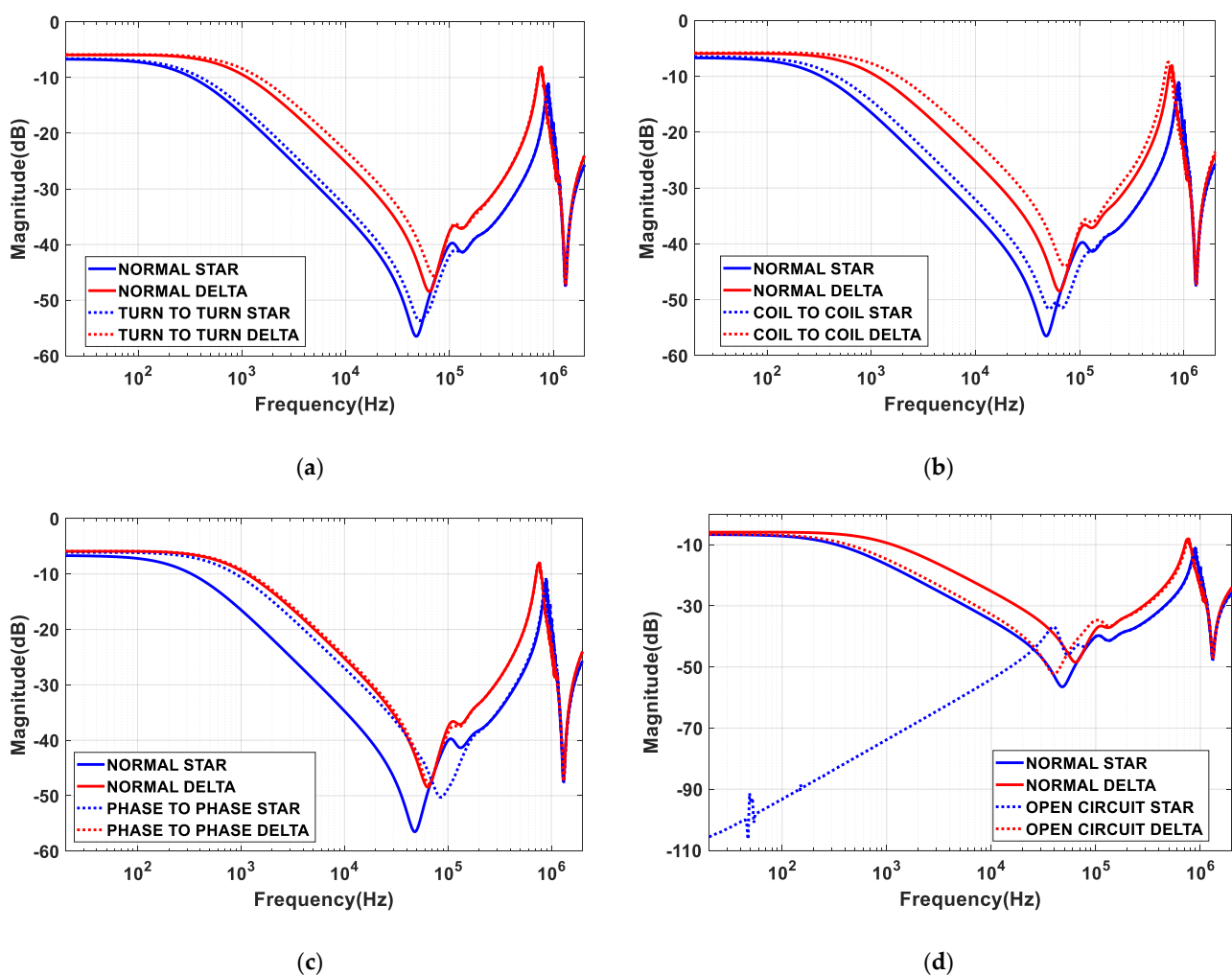


Figure 5. FRA measured responses for star vs. delta 5.5-IM at (a) Normal vs. Turn-to-Turn, (b) Normal vs. Coil-to-Coil, (c) Normal vs. Phase-to-Phase SC fault and (d) Normal vs. open circuit.

In Figure 5b, the Coil-to-Coil fault FRA patterns show a huge decrease in the response magnitude in the frequency range from 1 kHz to 1 MHz for the delta connection, while this variation is in frequencies from 100 kHz to 200 kHz for the star connection.

For the Phase-to-Phase faults shown in Figure 5c, a substantial variation in the response for the star connection in the frequency range from 20 Hz to 300 kHz can be noticed. On the other hand, the FRA patterns for the delta connection show a minor deviation in the response magnitude from the frequency from 1 kHz to 100 kHz.

Figure 5d shows a similar effect for the open-circuit fault on the star and delta windings as those in the above cases. The variation is noticeable in the frequency ranges from 20 Hz to 50 kHz for the star winding and from 100 Hz to 100 kHz for the delta winding.

4. Results Analysis

One of the research objectives is to analyse the IMs FRA patterns of the normal vs. SC and OC faults using advanced statistical indicators and artificial intelligence. It is well understood that indicators can compute the error ratio between two datasets. However, there are differences between one indicator to another in terms of the sensitivity. In the FRA of power transformers, statistical indicators are used to calculate the variations between two responses, i.e., the normal and faulty FRA signatures. The calculation is usually performed in three different FRA regions, according to the standard procedures [12]. Three frequency sub-bands: low frequency (LF), mid-frequency (MF) and high frequency (HF), are identified based on the effect of the core, the interaction between the windings, and the effect of the wiring, bushing and external leads. However, this frequency division is not applied to the IMs FRA signature. Therefore, in this paper, the frequency spectrum of the IM FRA signature is divided based on the equivalent electrical circuit parameters [32]. Based on the analogue principle, the FRA analyzer can plot the impedance $Z(R, L, C)(\omega)$, as presented in Figure 6.

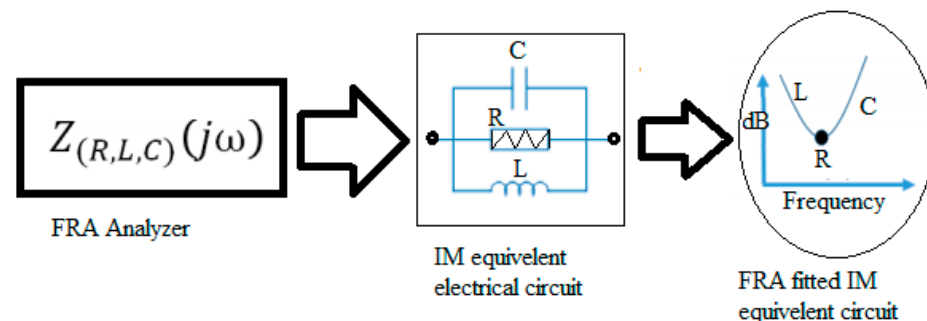


Figure 6. FRA of an equivalent IM RLC electrical circuit.

The above FRA signatures show that in the LF range (from 10 Hz to 1 kHz), the trend is a horizontal line (Figure 7a), where the resistive elements dominate the response. In the MF range (from 1 kHz to 60 kHz), the FRA trace exhibits a negative slope, as shown in Figure 7b. This range is mainly dominated by inductive elements. Within the HF range from 60 kHz to 1 MHz, as shown in Figure 7c, the capacitive elements present a positive slope in relation to the IM winding characteristics. A frequency response that is above 1 MHz is related to the effects of bushings and external leads. Thus, three frequency regions for the IM FRA studies are proposed, as shown in Figure 8.

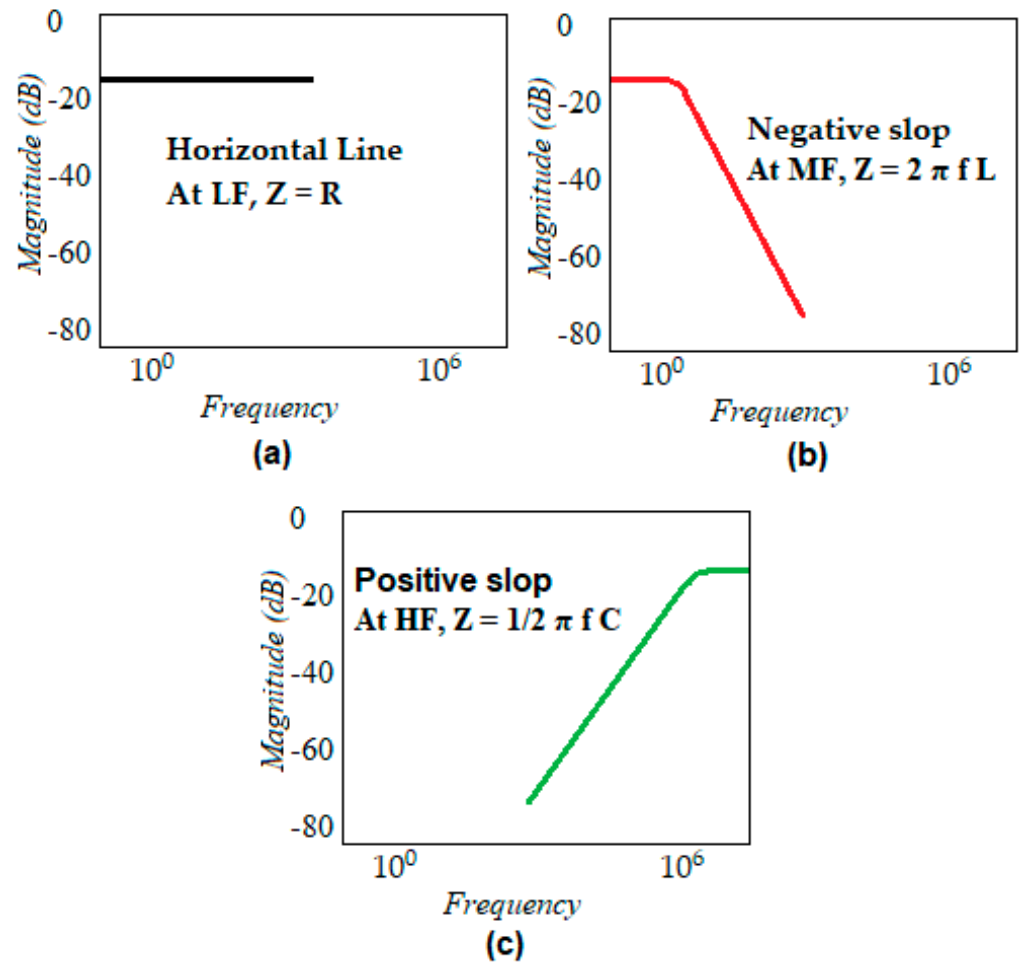


Figure 7. RLC parameters and their contribution to the measured FRA. (a) LF range (from 10 Hz to 1 kHz), (b) MF range (from 1 kHz to 60 kHz), (c) HF range (from 60 kHz to 1 MHz).

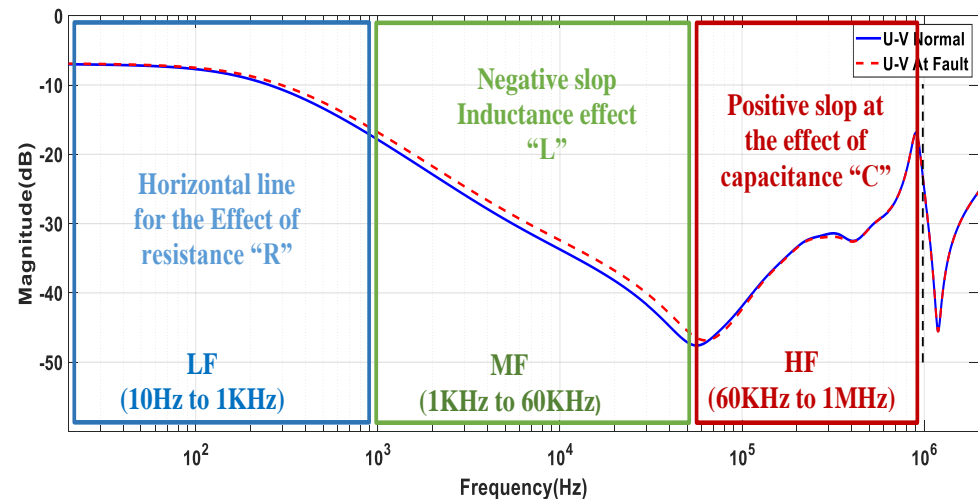


Figure 8. The proposed FRA sub-bands for IM FRA studies.

The calculated statistical indicators, along with their sensitivity analyses results, are listed in Figures 9–12. In this study, CC, SD, ASLE and MSE are used to compute the variation between the normal and faulty FRA signatures for the above three case studies. The results are analysed using the heatmapping color scaling using the minimum scaled values.

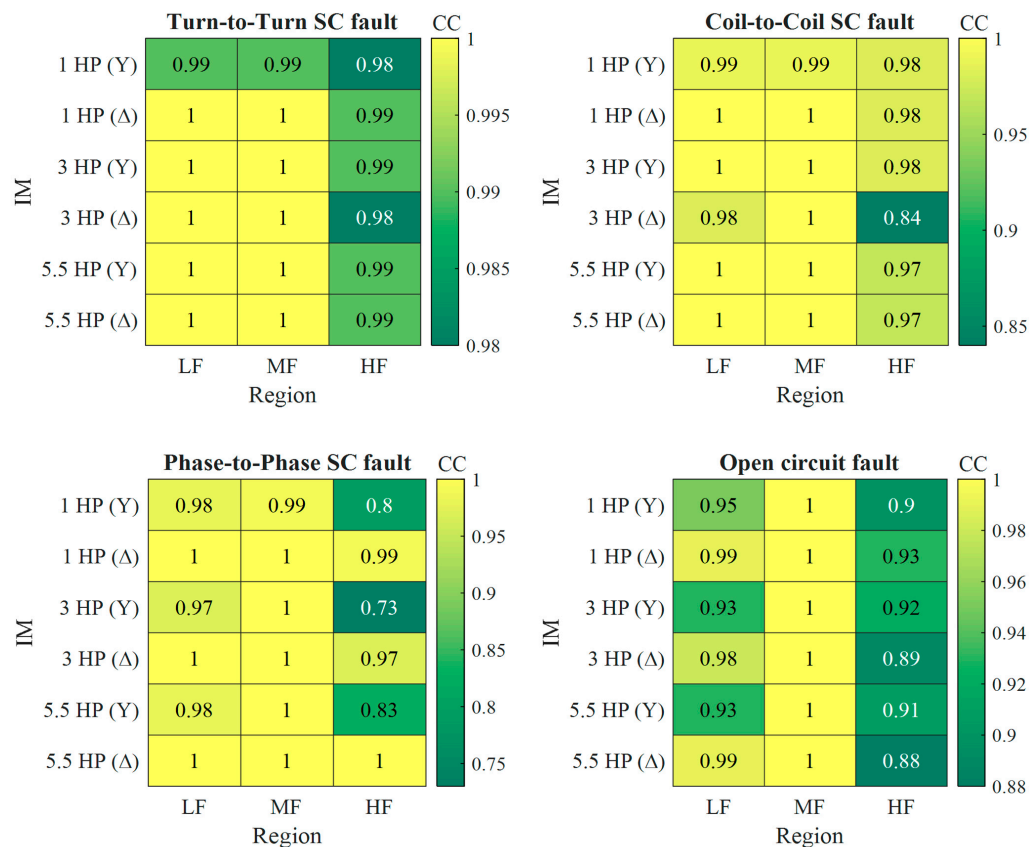


Figure 9. The CC calculated values between the normal and other faults.

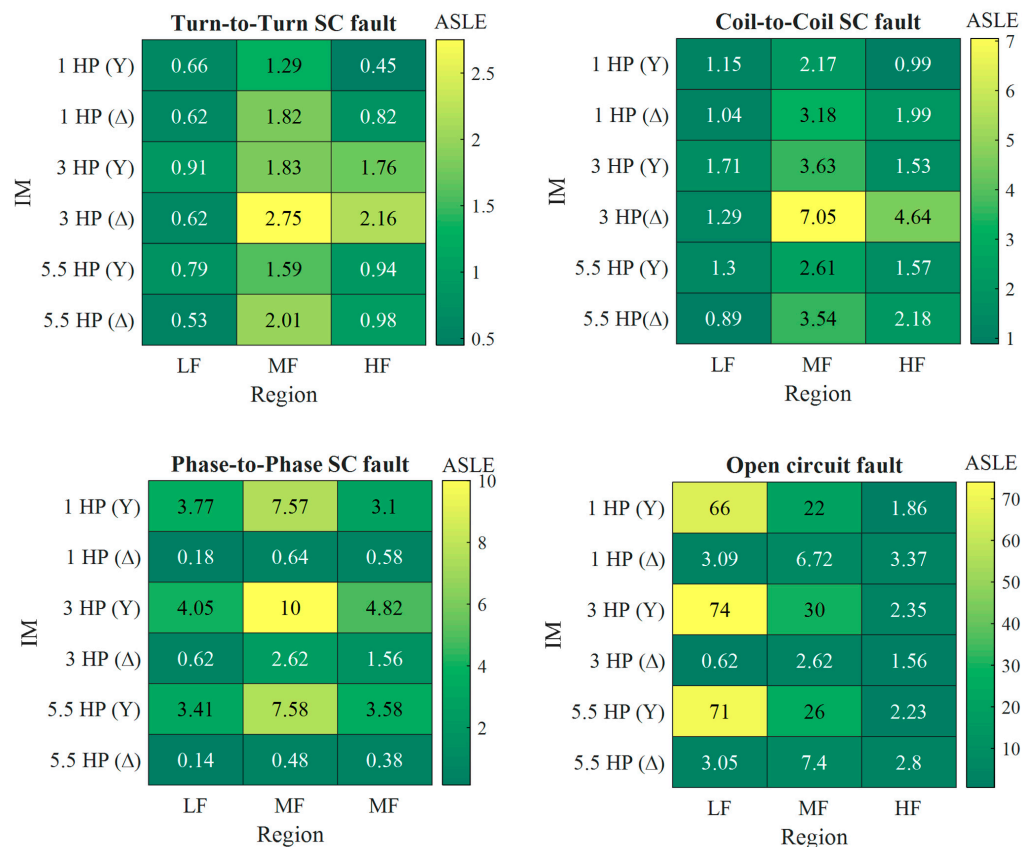


Figure 10. ASLE calculated values between normal and other faults.

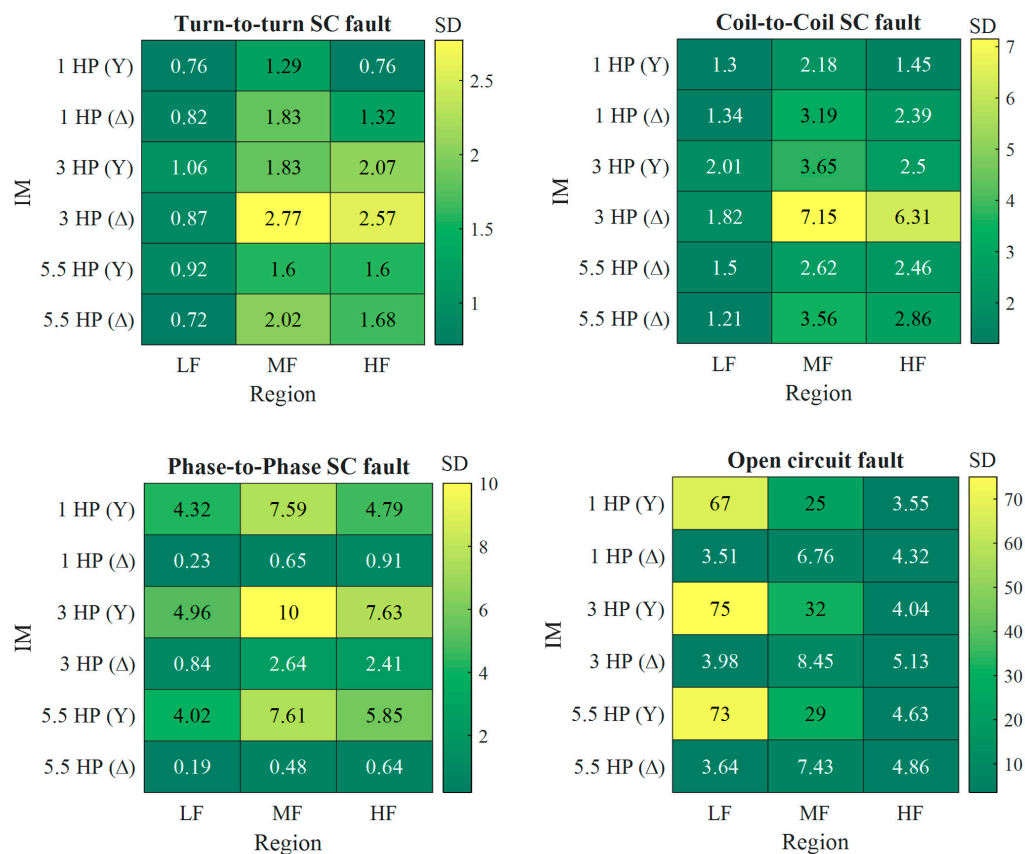


Figure 11. SD calculated values between normal and other faults.

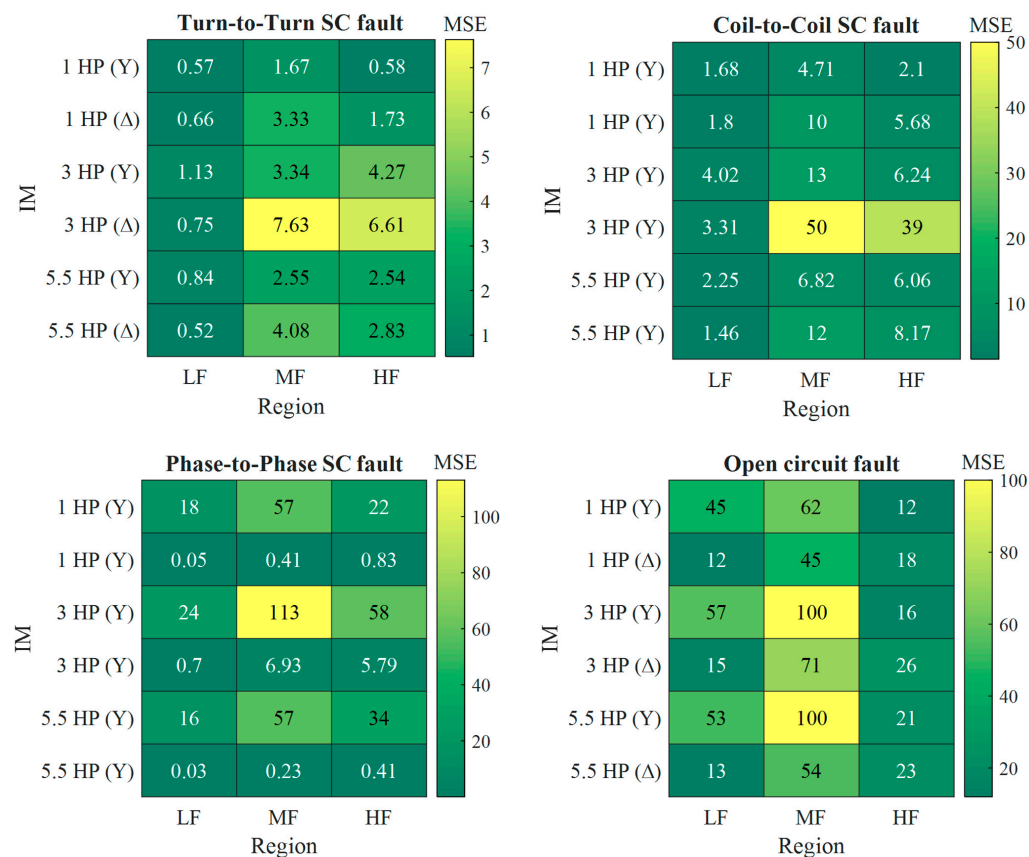


Figure 12. MSE calculated values between normal and other faults.

The CC values are presented in Figure 9. The CC is 1 when there is overlapping between the compared datasets, and the results are presented in a bright yellow color. The variation when we were calculating values of less than 0.98 are indicated by the green dark color. The CC values indicate that there is an overlapping between the normal and Turn-to-Turn faults in all of the frequency regions, but not for the 1 HP Y-connected HF region and the 3 HP Δ -connected HF region. For the Coil-to-Coil SC fault, the LF and MF regions overlap between the two signatures, but the value of CC is less than 0.98 in the HF region. The CC values for the Phase-to-Phase SC and OC faults are close to 1 in the MF region.

The CC in Equation (3) is less than 0.98 at the LF region for the 3 HP Y-connected IM when the Phase-to-Phase fault occurs. The CC indicates values of less than 0.98 at the HF regions for the Coil-to-Coil, Phase-to-Phase and open-circuit faults.

$$CC_{(X,Y)} = \frac{\sum_{i=1}^N X(i) \times Y(i)}{\sqrt{\sum_{i=1}^N [X(i)]^2 \times \sum_{i=1}^N [Y(i)]^2}} \quad (3)$$

The ASLE value in Equation (4) can display the variation between the two datasets when its value is above 1.5 [33]. In this study, the ASLE values indicate the variation when the calculated value is higher, as indicated by the bright yellow color in Figure 10. The ASLE indicates variation in the LF region for the Turn-to-Turn SC fault and in the HF region for the 3 HP IM. The ASLE also indicates values of above 1.5 in the MF and HF regions for the Coil-to-Coil fault, while it only indicates that in the LF region for the 3 HP Y-connected IM. For the Phase-to-Phase SC fault, the ASLE shows huge values of above 3.10 for the Y-connected IM. The ASLE values for the Δ connection are below 1.5 only in MF and HF regions for the 3 HP Δ -connected IM. Eventually, the ASLE shows huge values in all of the FRA regions for the OC fault.

$$ASLE_{(X,Y)} = \frac{\sum_{i=1}^N |20\log_{10} Y_i - 20\log_{10} X_i|}{N} \quad (4)$$

For the SD indicator in Equation (5), values of above 1.5 reveal a variation between the two datasets [34,35]. The calculated values for the SD indicator for the above case studies are shown in Figure 11. The bright and yellow colors present the detected variation. The SD indicates variation between the normal and Turn-to-Turn faults in the MF and HF regions, while it does not detect variation for the 1 HP Y-connected and Δ -connected IM in the HF region. The SD can show the variation between the normal and Coil-to-Coil faults in all of the regions, but it does not detect variations in LF for the 1 HP and 5.5 HP Δ -connected IMs. The SD values are above 1.5 in all of the regions for Phase-to-Phase SC fault for the IMs with a Y connection, whereas it is above 1.5 for the 3 HP Δ -connected IM in the MF and HF regions. The SD shows a huge value of above 3.5 for the OC fault in all of the FRA regions.

$$SD_{(X,Y)} = \sqrt{\frac{\sum_{i=1}^N [Y(i) - X(i)]^2}{N - 1}} \quad (5)$$

The MSE in Equation (6) shows a mostly similar trend to that of the SD, as can be seen from its values that is shown in Figure 12. It can be observed that the MSE shows higher values in the affected regions. Compared to the SD, the MSE in the 1 HP LF region for the Coil-to-Coil SC faults indicates values of above 1.5.

$$MSE = \frac{\sum_{i=1}^N (Y(i) - X(i))^2}{N} \quad (6)$$

5. Comparison of Star and Delta FRA Patterns

The FRA measurement shows a significant deviation between the Y winding and Δ winding FRA patterns for the normal and SC and OC faults. In all of the studied IMs and

in normal conditions, the Δ winding connection FRA signature magnitude reduces, and the first resonance frequency shifts to the higher frequencies compared to that for the Y winding connection. For example, in the 5.5 HP IM, the large negative spike magnitude reduced from -50 dB to -49 dB, and it shifted from 50 kHz to 70 kHz. For the Turn-to-Turn and the Coil-to-Coil SC faults, the effect shows similar FRA patterns for the Y- and Δ -connected IMs. The Phase-to-Phase fault presents different FRA patterns in the Y winding than it does in the Δ winding.

For the OC mechanism that is shown in Figure 13, the OC effect on the measured FRA is different in the Y winding connection to that in the Δ winding connection. Unlike the Y winding connection, the Δ winding connection current can flow from point “a” to point “c” through point “b”. Therefore, in terms of the effect of the OC on Δ , the winding connection did not show major variations compared to those of the Y winding connection.

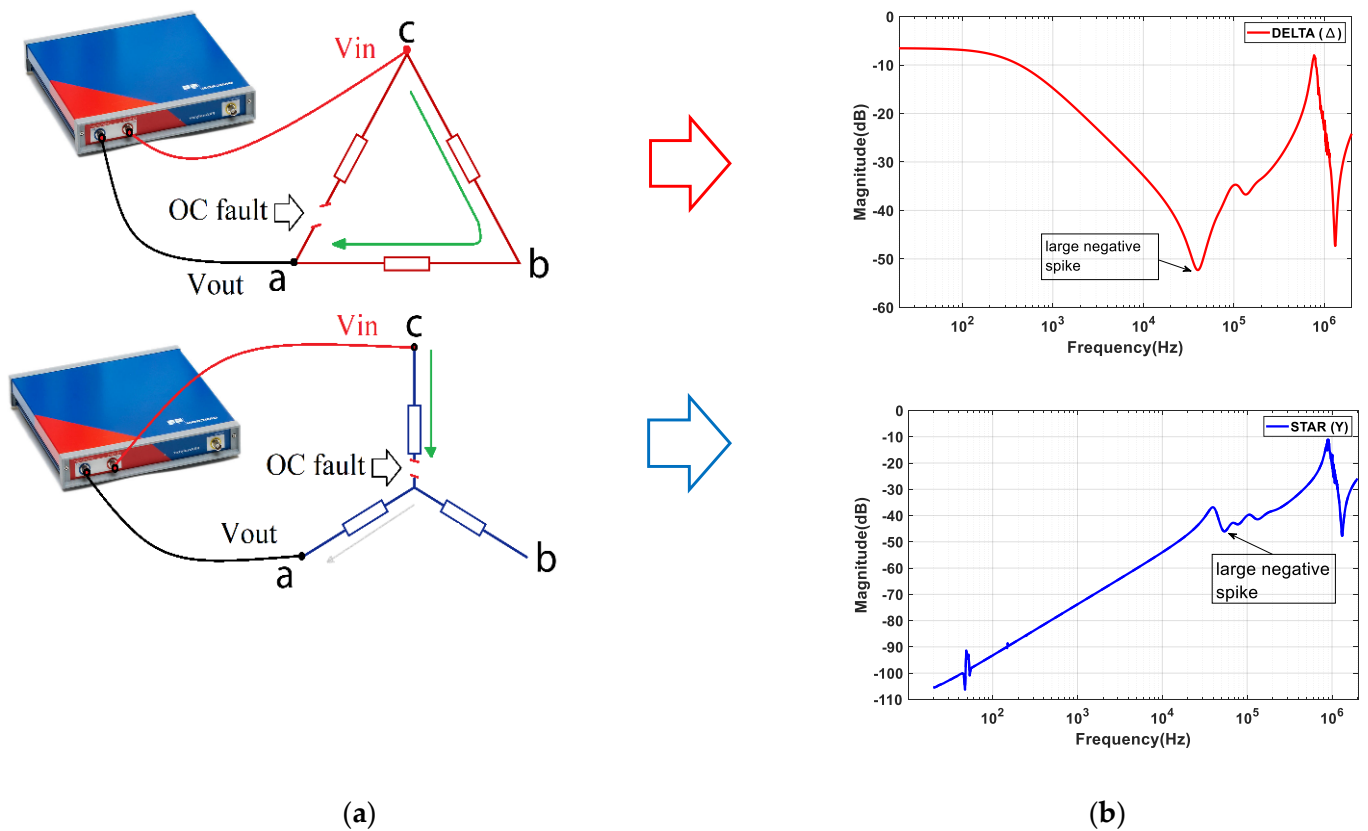


Figure 13. Mechanism of the OC fault and effect on FRA patterns. (a) Measurement connection. (b) FRA patterns.

Table 2 lists the three investigated IMs and the associated changes in the FRA patterns due to the IM winding connections and the developed SC and OC faults. This shows that the IMs winding connection affects the FRA signature.

Table 2. General comparison of the FRA measurement patterns of (Y) and (Δ) in normal and fault conditions.

Motor Model	Normal	Turn-to-Turn SC Fault	Coil-to-Coil SC Fault	Phase-to-Phase SC Fault	Open-Circuit Fault
1 HP		The fault causes a reduction of the response magnitude at the MF region. This effect is similar in both the Y winding connection and Δ winding connection.	The fault causes a reduction of magnitude in the LF and MF regions. This effect is similar in both the Y winding connection and Δ winding connection. However, it is not similar in the HF region. The Y winding connection shows the magnitude reduction from 100 kHz to 500 kHz.	The fault shows a small reduction of the magnitude in the MF and HF regions for Δ winding connection. However, for the Y winding connection, there is a huge reduction of the response magnitude in the LF, MF and HF regions.	
3 HP	Under normal conditions, the response magnitude (dB) reduces for the Y winding connection compared to that for the Δ winding connection. This is observed in all of the measured motors.	The fault causes a reduction of the response magnitude in the MF and HF regions. This effect is similar in both the Y winding connection and Δ winding connection.	The fault has a similar effect in LF and MF regions. There is a reduction of the response magnitude. There is a reduction of magnitude in the Δ winding connection in the HF region, but the fault did not show any effect at the HF region for the Y winding connection.	The fault shows a small reduction of the response magnitude at the MF region for Δ winding connection. On the other hand, the fault shows a huge reduction of the response magnitude in the LF, MF and HF regions for the Y winding connection.	The fault shows a small reduction of the response magnitude at LF and MF regions for Δ winding connection. The fault shows a huge reduction of the response magnitude at the LF region for Y winding reduction.
5.5 HP		The fault causes a reduction of the response magnitude at the MF region. This effect is similar in both the Y winding connection and Δ winding connection.	Similar effect to that in the 3 HP IM.	Similar effect to that in the 3 HP IM.	

In Table 2, the FRA measurement shows that under the normal condition, the response magnitude exposes a reduction of the Y winding connection compared to that in the Δ winding connection. This observation occurred in all of the measured motors. This reduction is due to the change in the winding geometries in the Y winding connection compared to that in the Δ winding connection. The Turn-to-Turn fault causes a reduction of the magnitude in the MF region for both the Y winding connection and Δ winding connection in 1 HP and 5.5 HP motors. The Turn-to-Turn fault causes a reduction of the magnitude in the MF and HF region for both the Y winding connection and Δ winding connection in the 3 HP motor. The Coil-to-Coil fault causes a reduction of the response magnitude in LF and MF regions in all of the motors at the Y winding connection and Δ winding connection. The Coil-to-Coil fault shows different effects in the HF region. The Coil-to-Coil fault shows the reduction of the magnitude for the Δ winding connection and Y winding connection for the 1 HP motor at 100 kHz to 500 kHz. The Coil-to-Coil fault does

not show the effect in the HF region for the 3 HP and 5.5 HP motors. The Phase-to-Phase fault shows a small reduction of the response magnitude in the MF and HF region for the Δ winding connection and a huge reduction of the response magnitude in the LF, MF and HF regions for the Y winding connection in the 1 HP motor. The Phase-to-Phase fault shows a small reduction of the response magnitude in the MF region for the Δ winding connection and a huge reduction of the response magnitude in the LF, MF and HF regions for the Y winding connection in the 3 HP and 5.5 HP motors. The open-circuit fault shows a small reduction of the response magnitude in the LF and MF regions for the Δ winding connection and a huge reduction or drop in the response magnitude in the LF region for the Y winding connection in all of the different motor sizes.

6. Conclusions

This paper presents a comprehensive analysis of the FRA patterns for the star and delta connections of three IMs of different sizes. The FRA patterns are measured for normal Y and Δ windings, which showed a similar trend, but there is a reduction of the case of the Δ winding. Under the fault conditions, a minor variation in the measured frequency response within the MF and HF ranges can be observed due to the Turn-to-Turn SC fault, and it shows a similar trend for the Y and Δ windings. The results also indicate that there is an average deviation between the normal and Coil-to-Coil SC faults in the MF and HF regions for the Y and Δ windings. There is a substantial variation in the MF and HF ranges due to the Phase-to-Phase SC fault for the Y winding. Unlike the Y winding, the Phase-to-Phase SC fault for the Δ winding shows an average deviation from the normal signature. A significant variation in the LF and MF regions is detected when the OC fault is implemented on the Y winding connection. On the other hand, an average variation is observed due to the OC implemented in the Δ winding connection. A further analysis is performed using CC, ASLE, SD and MSE. The employed indicators show that the ASLE, SD and MSE exhibit a good level of sensitivity to detect the error ratio between the normal and faulty FRA signatures. This paper considers the CC to be a second level that can be used to measure the FRA difference between the normal and faulty FRA signatures of IMs. The FRA patterns presented in this study can be used in the formulation of standard codes for IMs FRA signature interpretation and fault detection applications.

Author Contributions: Conceptualization, S.M.A.-A., M.F.M.Y. and A.A.-S.; methodology, S.M.A.-A. and A.A.A.; software, S.M.A.-A., A.A.S. and H.A.T.; validation, S.M.A.-A. and M.F.M.Y.; investigation, S.M.A.-A. and Z.A.-M.; resources, S.M.A.-A. and M.F.M.Y.; writing—original draft preparation, S.M.A.-A.; writing review and editing, M.F.M.Y., A.A.S., A.A.-S. and M.I.M.; A.A.A., H.A.T. and Z.A.-M.; Project administration: Z.A.N. and M.I.M. All authors have read and agreed to the published version of the manuscript.

Funding: This research was funded by the Ministry of Higher Education Malaysia, under the Fundamental Research Grant Scheme Nos 06E12, 4B482, 05G88, and 05G89, and The Islamic University, Najaf, Iraq.

Data Availability Statement: The data presented in this study are available in this article.

Acknowledgments: The authors gratefully acknowledge the Malaysia Ministry of Education and Universiti Teknologi Malaysia for funding this research with grants (nos 06E12, 4B482, 05G88, and 05G89). The authors would like to thank Mohd Aizam Talib from TNB Lab Malaysia for his assistance during the experiment. We would also like to thank all the subjects who volunteered to participate in this study.

Conflicts of Interest: The authors declare no conflict of interest.

References

1. Motor Reliability Working Group. Report of Large Motor Reliability Survey of Industrial and Commercial Installations, Part I. *IEEE Trans. Ind. Appl.* **1985**, *IA-21*, 853–864. [[CrossRef](#)]
2. Cornell, P.F.E.P.; Owen, E.L.; Appiarius, J.C.; McCoy, R.M.; Albrecht, D.W.H. *Improved Motors for Utility Applications*; Final Report; General Electric Company: Schenectady, NY, USA, 1982.

3. Florkowski, M.; Florkowska, B.; Zydron, P. Partial discharges in insulating systems of low voltage electric motors fed by power electronics—Twisted-pair samples evaluation. *Energies* **2019**, *12*, 768. [[CrossRef](#)]
4. Sakhalkar, N.P.; Korde, P. Fault detection in induction motors based on motor current signature analysis and accelerometer. In Proceedings of the 2017 International Conference on Energy, Communication, Data Analytics and Soft Computing (ICECDS), Chennai, India, 1–2 August 2017; pp. 363–367. [[CrossRef](#)]
5. Sonje, D.M.; Kundu, P.; Chowdhury, A. A Novel Approach for Sensitive Inter-turn Fault Detection in Induction Motor under Various Operating Conditions. *Arab. J. Sci. Eng.* **2019**, *44*, 6887–6900. [[CrossRef](#)]
6. Chen, P.; Xie, Y.; Hu, S. Electromagnetic Performance and Diagnosis of Induction Motors with Stator Interturn Fault. *IEEE Trans. Ind. Appl.* **2021**, *57*, 1354–1364. [[CrossRef](#)]
7. Gyftakis, K.N.; Cardoso, A.J.M. Reliable Detection of Stator Interturn Faults of Very Low Severity Level in Induction Motors. *IEEE Trans. Ind. Electron.* **2021**, *68*, 3475–3484. [[CrossRef](#)]
8. Kumar, A.; Bhalja, B.R.; Kumbhar, G.B. Novel Technique for Location Identification and Estimation of Extent of Turn-to-Turn Fault in Transformer Winding. *IEEE Trans. Ind. Electron.* **2022**, 1–10. [[CrossRef](#)]
9. Abu-Siada, A.; Hashemnia, N.; Islam, S.; Masoum, M. Understanding Power Transformer Frequency Response Analysis Signatures. *IEEE Electr. Insul. Mag.* **2013**, *29*, 48–56. [[CrossRef](#)]
10. Picher, P. Mechanical Condition Assessment of Transformer Windings Using Frequency Response Analysis (Fra). *Cigre Eval.* **2008**, *A2.26*, 30–34.
11. IEC 60076-18 Ed.1; Power Transformers—Part 18, ‘Measurement of Frequency Response’. International Electrotechnical Commission: Geneva, Switzerland, 2012.
12. IEEE Std C57.149-2012; IEEE Guide for the Application and Interpretation of Frequency Response Analysis for Oil-Immersed Transformers IEEE Power and Energy Society. IEEE: Piscataway, NJ, USA, 2013; pp. 1–72. [[CrossRef](#)]
13. Cheng, B.; Wang, Z.; Crossley, P. Using Lumped Element Equivalent Network Model to Derive Analytical Equations for Interpretation of Transformer Frequency Responses. *IEEE Access* **2020**, *8*, 179486–179496. [[CrossRef](#)]
14. Al-Ameri, S.M.; Kamarudin, M.S.; Yousof, M.F.M.; Salem, A.A.; Siada, A.A.; Mosaad, M.I. Interpretation of Frequency Response Analysis for Fault Detection in Power Transformers. *Appl. Sci.* **2021**, *11*, 2923. [[CrossRef](#)]
15. Uhrig, S.; Ottl, F.; Hinterholzer, R.; Augeneder, N. Reliable Diagnostics on Rotating Machines using FRA. In Proceedings of the 2020 International Conference on Diagnostics in Electrical Engineering (Diagnostika), Pilsen, Czech Republic, 1–4 September 2020. [[CrossRef](#)]
16. Yousof, M.F.M.; Alawady, A.A.; Al-Ameri, S.M.; Azis, N.; Illias, H.A. FRA Indicator Limit for Faulty Winding Assessment in Rotating Machine. In Proceedings of the 2021 IEEE International Conference on the Properties and Applications of Dielectric Materials (ICPADM), Johor Bahru, Malaysia, 12–14 July 2021; Volume 2021-July, pp. 346–349. [[CrossRef](#)]
17. Vilhekar, T.G.; Ballal, M.S.; Umre, B.S. Application of Sweep Frequency Response Analysis for the detection of winding faults in induction motor. In Proceedings of the IECON 2016—42nd Annual Conference of the IEEE Industrial Electronics Society, Florence, Italy, 23–26 October 2016; pp. 1458–1463. [[CrossRef](#)]
18. Alawady, A.A.; Yousof, M.F.M.; Azis, N.; Talib, M.A. Frequency response analysis technique for induction motor short circuit faults detection. *Int. J. Power Electron. Drive Syst.* **2020**, *11*, 1653–1659. [[CrossRef](#)]
19. Alawady, A.A.; Yousof, M.F.M.; Azis, N.; Talib, M.A. Phase to phase fault detection of 3-phase induction motor using FRA technique. *Int. J. Power Electron. Drive Syst.* **2020**, *11*, 1241–1248. [[CrossRef](#)]
20. Brandt, M.; Kascak, S. Failure identification of induction motor using SFRA method. In Proceedings of the ELEKTRO 2016—11th International Conference, Strbske Pleso, Slovakia, 16–18 May 2016; pp. 269–272. [[CrossRef](#)]
21. Brandt, M.; Gutten, M.; Kaščák, S. Diagnostic of induction motor using SFRA method. In Proceedings of the 2016 Conference on Diagnostics in Electrical Engineering (Diagnostika), Pilsen, Czech Republic, 6–8 September 2016. [[CrossRef](#)]
22. Yu, Y.; Zhao, Z.; Chen, Y.; Wu, H.; Tang, C.; Gu, W. Evaluation of the Applicability of IFRA for Short Circuit Fault Detection of Stator Windings in Synchronous Machines. *IEEE Trans. Instrum. Meas.* **2022**, *71*, 1–12. [[CrossRef](#)]
23. Samimi, M.H.; Tenbohlen, S.; Akmal, A.A.S.; Mohseni, H. Evaluation of numerical indices for the assessment of transformer frequency response. *IET Gener. Transm. Distrib.* **2017**, *11*, 218–227. [[CrossRef](#)]
24. Al-Ameri, S.M.A.N.; Kamarudin, M.S.; Yousof, M.F.M.; Salem, A.A.; Banakhr, F.A.; Mosaad, M.I.; Abu-Siada, A. Understanding the Influence of Power Transformer Faults on the Frequency Response Signature Using Simulation Analysis and Statistical Indicators. *IEEE Access* **2021**, *9*, 70935–70947. [[CrossRef](#)]
25. Sant’Ana, W.C.; Salomon, C.P.; Lambert-Torres, G.; da Silva, L.E.B.; Bonaldi, E.L.; de Oliveira, L.E.D.L.; da Silva, J.G.B. A survey on statistical indexes applied on frequency response analysis of electric machinery and a trend based approach for more reliable results. *Electr. Power Syst. Res.* **2016**, *137*, 26–33. [[CrossRef](#)]
26. Ukil, A.; Chen, S.; Andenna, A. Detection of stator short circuit faults in three-phase induction motors using motor current zero crossing instants. *Electr. Power Syst. Res.* **2011**, *81*, 1036–1044. [[CrossRef](#)]
27. Yousof, M.F.M.; Al-Ameri, S.; Ahmad, H.; Illias, H.A.; Arshad, S.N.M. A new approach for estimating insulation condition of field transformers using FRA. *Adv. Electr. Comput. Eng.* **2020**, *20*, 35–42. [[CrossRef](#)]
28. Sultanbek, A. Exploring Statistical Index Criteria for Transformer Frequency Response Interpretation. Master’s Thesis, Nazarbayev University, Astana, Kazakhstan, 2018.

29. Kim, J.-W.; Park, B.; Jeong, S.C.; Kim, S.W.; Park, P. Fault Diagnosis of a Power Transformer Using an Improved Frequency-Response Analysis. *IEEE Trans. Power Deliv.* **2005**, *20*, 169–178. [[CrossRef](#)]
30. Bramerdorfer, G.; Tapia, J.A.; Pyrhönen, J.J.; Cavagnino, A. Modern Electrical Machine Design Optimization: Techniques, Trends, and Best Practices. *IEEE Trans. Ind. Electron.* **2018**, *65*, 7672–7684. [[CrossRef](#)]
31. Orosz, T.; Rassölkin, A.; Kallaste, A.; Arsénio, P.; Pánek, D.; Kaska, J.; Karban, P. Robust Design Optimization and Emerging Technologies for Electrical Machines: Challenges and Open Problems. *Appl. Sci.* **2020**, *10*, 6653. [[CrossRef](#)]
32. Mugarra, A.; Mayora, H.; Guerrero, J.M.; Platero, C.A. Frequency Response Analysis (FRA) Fault Diagram Assessment Method. *IEEE Trans. Ind. Appl.* **2022**, *58*, 336–344. [[CrossRef](#)]
33. Badgajar, K.P.; Maoyafikuddin, M.; Kulkarni, S.V. Alternative statistical techniques for aiding SFRA diagnostics in transformers. *IET Gener. Transm. Distrib.* **2012**, *6*, 189–198. [[CrossRef](#)]
34. Secue, J.R.; Mombello, E. Sweep frequency response analysis (SFRA) for the assessment of winding displacements and deformation in power transformers. *Electr. Power Syst. Res.* **2008**, *78*, 1119–1128. [[CrossRef](#)]
35. Behjat, V.; Mahvi, M. Statistical approach for interpretation of power transformers frequency response analysis results. *IET Sci. Meas. Technol.* **2015**, *9*, 367–375. [[CrossRef](#)]

Disclaimer/Publisher’s Note: The statements, opinions and data contained in all publications are solely those of the individual author(s) and contributor(s) and not of MDPI and/or the editor(s). MDPI and/or the editor(s) disclaim responsibility for any injury to people or property resulting from any ideas, methods, instructions or products referred to in the content.